

---

This is an electronic reprint of the original article.  
This reprint may differ from the original in pagination and typographic detail.

Eik, Marika; Papenfuss, Christina

## Velocity gradients of concrete mass reconstructed based on measured fibre orientations in hardened concrete

*Published in:*  
Composite Structures

*DOI:*  
[10.1016/j.compstruct.2019.111008](https://doi.org/10.1016/j.compstruct.2019.111008)

Published: 01/10/2019

*Document Version*  
Peer-reviewed accepted author manuscript, also known as Final accepted manuscript or Post-print

*Published under the following license:*  
CC BY-NC-ND

*Please cite the original version:*  
Eik, M., & Papenfuss, C. (2019). Velocity gradients of concrete mass reconstructed based on measured fibre orientations in hardened concrete. *Composite Structures*, 225, Article 111008.  
<https://doi.org/10.1016/j.compstruct.2019.111008>

---

This material is protected by copyright and other intellectual property rights, and duplication or sale of all or part of any of the repository collections is not permitted, except that material may be duplicated by you for your research use or educational purposes in electronic or print form. You must obtain permission for any other use. Electronic or print copies may not be offered, whether for sale or otherwise to anyone who is not an authorised user.

## Accepted Manuscript

Velocity gradients of concrete mass reconstructed based on measured fibre orientations in hardened concrete

Marika Eik, Christina Papenfuss

PII: S0263-8223(19)30537-9  
DOI: <https://doi.org/10.1016/j.compstruct.2019.111008>  
Article Number: 111008  
Reference: COST 111008

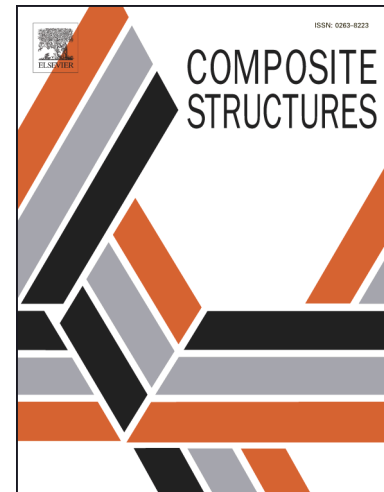
To appear in: *Composite Structures*

Received Date: 1 February 2019

Accepted Date: 20 May 2019

Please cite this article as: Eik, M., Papenfuss, C., Velocity gradients of concrete mass reconstructed based on measured fibre orientations in hardened concrete, *Composite Structures* (2019), doi: <https://doi.org/10.1016/j.compstruct.2019.111008>

This is a PDF file of an unedited manuscript that has been accepted for publication. As a service to our customers we are providing this early version of the manuscript. The manuscript will undergo copyediting, typesetting, and review of the resulting proof before it is published in its final form. Please note that during the production process errors may be discovered which could affect the content, and all legal disclaimers that apply to the journal pertain.



# Velocity gradients of concrete mass reconstructed based on measured fibre orientations in hardened concrete

Marika Eik<sup>a</sup>, Christina Papenfuss<sup>b,\*</sup>

<sup>a</sup> *Civil Engineering Department, Aalto University School of Engineering, Rakentajanaukio 4 A, Otaniemi, 02150 Espoo Finland*

<sup>b</sup> *Hochschule für Technik und Wirtschaft, Berlin HTW - University of Applied Sciences, Wilhelminenhofstr. 75 A, 12459 Berlin, Germany*

---

## Abstract

During the casting of steel fibre reinforced concrete (SFRC) the orientation of fibres is influenced by flow dynamics of concrete mass. A simple theoretical model presented allows the calculation of velocity gradient matrices for concrete mass based on steel fibre orientations measured in the hardened concrete samples taken from the different regions in the slabs. This made it possible to examine the realistic trends of the flow near the formwork or free surface or in the bulk material. Eigenvalues and eigenvectors of the matrices show the directions of the maximal and minimal velocity changes, which can be compared in different positions of the slabs. The outcomes of the study can contribute to controlled production technology of SFRC.

*Keywords:* fibres, reinforced cement/plaster, anisotropy, rheological properties

---

## 1. Introduction

Fibre reinforced composites become more and more important in many fields of application: carbon or glass fibres are introduced into polymers in order to increase the strength, see f.i. [2, 3]. The mechanical properties of a fibre reinforced composite depend on fibre orientations, see f.i. [1] for a prediction of fibre orientations and distributions and [4] for a constitutive model. During the flow process the flow field and fibre orientations influence each other [5]. This effect is well known for different kind of fibre suspensions, like f.i. polystyrene

---

\*Corresponding author. Tel.: +49 30 5019-3203

*Email addresses:* marika.eik@aalto.fi (Marika Eik),  
Christina.Papenfuss@htw-berlin.de (Christina Papenfuss )

melt with carbon nano-fibres and others [6, 7, 8, 9, 10]. Theoretical models have been developed to account for flow induced orientational order and shear thinning in fibre suspensions.

In civil engineering short steel fibres are added to concrete mass to increase the tensile strength and to decrease brittle failure characteristics of the final composite. During the filling process of steel fibre reinforced concrete (SFRC) the orientation of fibres is defined by the flow properties of concrete mass, and when the mass is set, the orientations are fixed and the orientation distribution of fibres is frozen.

With the present paper we would like to demonstrate the preferential tendencies of SFRC mass during the casting based on the velocity gradient matrices reconstructed using the measured orientation distributions of fibres in hardened state of concrete. The advantage of the approach presented is its simplicity, meaning that solving of the coupled differential equations for the velocity field and fibre orientation is avoided. This would be possible only numerically, and the question of boundary conditions at the solid interface of the formwork and at the free surface had to be investigated. The orientation of fibres used in the study was measured by x-ray micro-computed tomography ( $\mu$ CT), whose accuracy is greater than other methods for measuring of fibre orientations [15]. The additional advantage of the study is that the reconstructed velocity gradient matrices take into account the measured fibre orientations in different regions of full-size floor-slabs, which makes it possible to examine the realistic trends of the flow front of concrete mass near the formwork or free surface or in the bulk material. The velocity gradient matrix varies depending on the flow dynamics of concrete mass making the measuring of fibre orientations in a flowing mass hardly feasible. In the study the velocity gradient matrices are calculated algebraically at the end phase of concrete mass flow, when a stationary state for fibre orientations is reached and the orientation distributions of fibres are frozen afterwards.

The outcomes of the study can contribute to controlled production technology of SFRC by giving an estimate f.i. for a casting technique, such as the effect of filling rate of concrete mass on the alignment of fibres close to boundary, free surface or in the bulk material, which is relevant for the properties of the final

composite.

## 2. Theoretical model

Orientation tensors are introduced as a measure of the anisotropy of the fibre orientations. The time evolution of the orientation tensors is coupled to the flow field. The theoretical model for the time derivative of the second order tensor adopted here goes back to Advani and Tucker [14]:

$$\begin{aligned} \frac{d\mathbf{O}^{(2)}}{dt} = & -\frac{1}{2} \left( \boldsymbol{\omega} \cdot \mathbf{O}^{(2)} - \mathbf{O}^{(2)} \cdot \boldsymbol{\omega} \right) + \\ & \frac{1}{2} \lambda \left( (\nabla \mathbf{v})^{sym} \cdot \mathbf{O}^{(2)} + \mathbf{O}^{(2)} \cdot (\nabla \mathbf{v})^{sym} - 2(\nabla \mathbf{v})^{sym} : \mathbf{O}^{(4)} \right) + \\ & 2D \left( \delta - 3\mathbf{O}^{(2)} \right), \end{aligned} \quad (1)$$

$\frac{d}{dt}$  denotes the material time derivative,  $\lambda$  is the aspect ratio of a fibre, and  $(\nabla \mathbf{v})^{sym}$  is the symmetric part of the velocity gradient. The orientation tensors of second and fourth orders are denoted by  $\mathbf{O}^{(2)}$  and  $\mathbf{O}^{(4)}$ . They are defined as the moments of the orientation distribution function:

$$\mathbf{O}^{(2)}(\mathbf{x}, t) = \int_{S^2} f(\mathbf{n}, \mathbf{x}, t) \mathbf{n} \mathbf{n} d^2 n \quad (2)$$

$$\mathbf{O}^{(4)}(\mathbf{x}, t) = \int_{S^2} f(\mathbf{n}, \mathbf{x}, t) \mathbf{n} \mathbf{n} \mathbf{n} \mathbf{n} d^2 n \quad (3)$$

The last term in equation (1) was introduced originally to account for the effect of orientation diffusion. If  $(\nabla \mathbf{v})^{sym} = 0$  then a term  $D$  leads to a decrease of the second order orientation tensor  $\mathbf{O}^{(2)}$  by making the distribution more isotropic (randomising effect). The interaction between fibres would make the distribution more anisotropic, whereas the interaction with aggregate will result in more isotropic (randomised) orientation distribution. Thereby, due to the size of steel fibres used (length in the range of centimetres), orientation diffusion is not important, but the interaction of fibres with aggregate is relevant. This randomising effect may be described as well by a term of the form  $2D(\delta - 3\mathbf{O}^{(2)})$  with the unit tensor  $\delta$ .

We assume, that the vorticity of the flow field (the anti-symmetric part of the velocity gradient) is zero ( $\boldsymbol{\omega} = 0$ ) and that the orientation tensor is stationary,  $\frac{d\mathbf{O}^{(2)}}{dt} = 0$ , meaning that fibre orientations correspond to the end

phase of mass flow and their orientation is frozen afterwards. Under these assumptions equation (1) simplifies to:

$$0 = \frac{1}{2}\lambda \left( \nabla \mathbf{v} \cdot \mathbf{O}^{(2)} + \mathbf{O}^{(2)} \cdot \nabla \mathbf{v} - 2\nabla \mathbf{v} : \mathbf{O}^{(4)} \right) + 2D \left( \delta - 3\mathbf{O}^{(2)} \right) \quad (4)$$

The components of the orientation tensors are obtained from the measurements of fibre orientations in hardened state of concrete by  $\mu$ CT, and equation (4) is solved for the components of the velocity gradient.

### 3. Orientation tensors based on the measured orientation distributions of fibres

The orientation distributions of fibres were measured in horizontal structural elements, i.e. six full-size floor-slabs [16]. The type of structure selected enabled to examine the orientation distribution of fibres close to the formwork and in the bulk material. The slabs were cast in a factory using a bucket (Figure 1(b)), following the scheme represented in Figure 2(a).



**Fig. 1.** Casting of full-size floor-slabs in a factory. (a) Representation of the formwork with surface treatment. (b) Representation of the way of casting.

The bottom of the formwork was polyetenfilm on concrete floor and no oil or other chemicals were added. The edge of the formwork were plywood film-coated and also no oil or other chemicals were added, since the plywood was new and was not used before. A class of concrete used was C30/37 with the largest aggregate size of 16 mm. A type was self compacting concrete (SCC), meaning that no vibration was needed. The fibres used were steel hooked-end with an aspect ratio of  $\frac{l_f}{d_f} = \frac{50}{1.0}$  and their amount per cubic meter of concrete was 88 kg, which made about 250 fibres per  $\text{dm}^3$ , (Figure 2(b)).

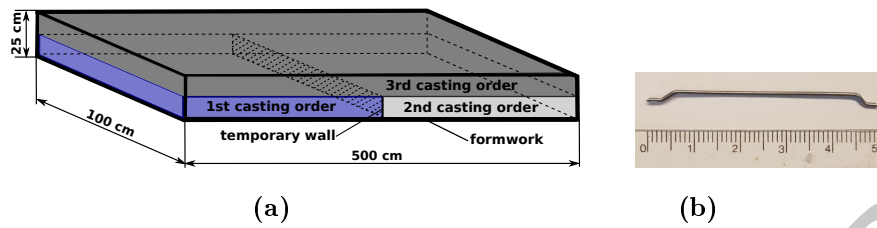


**Fig. 2.** (a) Casting order of full-size floor-slabs. (b) Used steel fibres with hooked-ends. The length of a fibre was  $l_f = 50$  mm and diameter was  $d_f = 1.0$  mm.

After curing for 28 days, the slabs were tested using a three point bending test. Three out of six slabs demonstrated approximately the same load-bearing capacity (slabs 1, 2, 3), while the capacity of the remaining slabs were lower [16, 17].

The orientation distributions of fibres in the tested floor-slabs were measured in cylindrical samples with a diameter of 10 cm, which were extracted from the slabs according to the scheme represented in Figure 3(a). Two cylinders were drilled from each slab; one from the side region to observe the effect of the vertical formwork (wall effect), and another one from the central region of a slab to measure fibre orientations in the bulk material (Figure 4). The cylinders extracted from the side region were marked as "A"-samples and from the central region as "B"-samples (Figure 3). Altogether there were 12 cylinders.

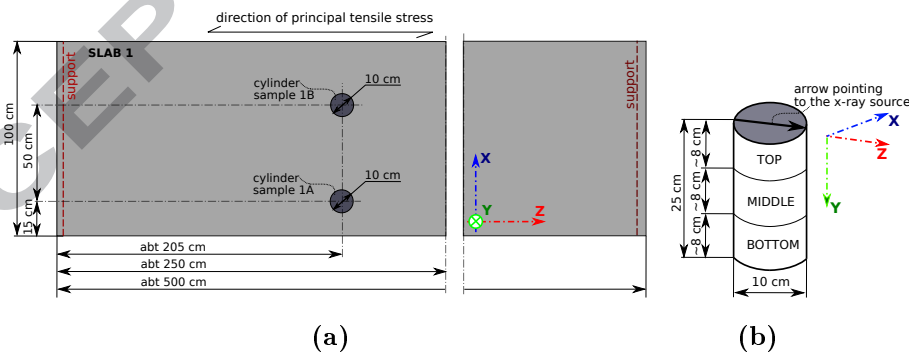


**Fig. 3.** (a) The position of cylinder samples in the floor-slabs. (b) Parts of a cylinder sample scanned by x-ray micro-tomography.

The orientation distributions of fibres were measured by  $\mu$ CT method, which allowed to represent the fibres directly in three-dimensions, and the application of the skeletonization algorithm gave the orientation of each individual fibre. All

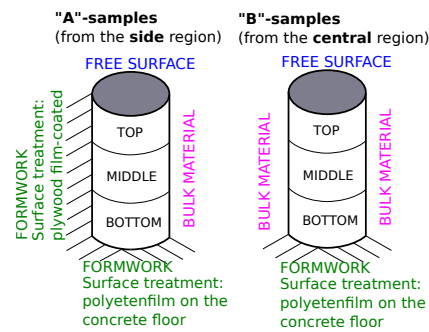


**Fig. 4.** Boundary conditions of extracted cylinders for estimating the velocity gradient matrices.

cylindrical samples were scanned in the middle part, which was equal to about 8 cm in cylinder height, and four cylinders were also scanned in the top and bottom parts (Figure 4). The height of the scanning area was conditioned by height of LCD detector and by intention to examine the effect of formwork, free surface and bulk material on the orientation distributions of fibres. The measured orientation distribution functions allowed to calculate the all orientation tensors of successive order [4, 16]. Here, the second and fourth order orientation tensors are involved, defined by equations (2) and (3).

#### 4. Velocity gradients of concrete mass based on measured fibre orientations in hardened state of concrete

Our model includes the following assumptions:

- The flow problem to solve is a steady state, meaning that concrete mass has reached the end phase of flow;
- Fibre orientation does not change during the setting/hardening time of concrete mass. The fibres can reorient during the flow process, but as soon as a setting of concrete mass begins the orientation of fibres is frozen and not change afterwards;
- The material parameter  $D$  in equation (1) is assumed to be constant;
- In case of (very liquid) SCC, the flow may become turbulent, see f.i. [18]. A single fibre in fresh concrete mass is reoriented by the local velocity

gradient, because both fibre ends experience different velocities. The orientation of a single fibre depends on the velocity gradient at the fibre position. The orientation of all steel fibres measured in the cylindrical sample means that the calculated velocity gradient is an average over the sample of 10 cm in diameter.

If the components of  $(\nabla \mathbf{v})^{symm}$  in equation (1) are denoted by  $\dot{\gamma}_{ij}$  then the equation reads (in Cartesian components) as follows:

$$\left. \begin{aligned}
 & (2O_{11} - 2O_{1111})\dot{\gamma}_{11} - 2O_{1122}\dot{\gamma}_{22} - 2O_{1133}\dot{\gamma}_{33} \\
 & + (2O_{12} - 4O_{1112})\dot{\gamma}_{12} + (2O_{13} - 4O_{1113})\dot{\gamma}_{13} - 4O_{1123}\dot{\gamma}_{23} \\
 & \qquad \qquad \qquad = -\frac{2D}{\lambda}(1 - 3O_{11}) \\
 & -2O_{2211}\dot{\gamma}_{11} + (2O_{22} - 2O_{2222})\dot{\gamma}_{22} - 2O_{2233}\dot{\gamma}_{33} + \\
 & (2O_{12} - 4O_{2212})\dot{\gamma}_{12} - 4O_{2213}\dot{\gamma}_{13} + (2O_{23} - 4O_{2223})\dot{\gamma}_{23} \\
 & \qquad \qquad \qquad = -\frac{2D}{\lambda}(1 - 3O_{22}) \\
 & -2O_{3311}\dot{\gamma}_{11} - 2O_{3322}\dot{\gamma}_{22} + (2O_{33} - 2O_{3333})\dot{\gamma}_{33} \\
 & -4O_{3312}\dot{\gamma}_{12} + (2O_{13} - 4O_{3313})\dot{\gamma}_{13} + (2O_{23} - 4O_{3323})\dot{\gamma}_{23} \\
 & \qquad \qquad \qquad = -\frac{2D}{\lambda}(1 - 3O_{33}) \\
 & (O_{12} - 2O_{1211})\dot{\gamma}_{11} + (O_{12} - 2O_{1222})\dot{\gamma}_{22} - 2O_{1233}\dot{\gamma}_{33} \\
 & + (O_{22} + O_{11} - 4O_{1212})\dot{\gamma}_{12} + (O_{32} - 4O_{1213})\dot{\gamma}_{13} + (O_{13} - 4O_{1223})\dot{\gamma}_{23} \\
 & \qquad \qquad \qquad = \frac{2D}{\lambda}3O_{12} \\
 & (O_{13} - 2O_{1311})\dot{\gamma}_{11} - 2O_{1322}\dot{\gamma}_{22} + (O_{13} - 2O_{1333})\dot{\gamma}_{33} \\
 & + (O_{23} - 4O_{1312})\dot{\gamma}_{12} + (O_{33} + O_{11} - 4O_{1313})\dot{\gamma}_{13} + (O_{12} - 4O_{1323})\dot{\gamma}_{23} \\
 & \qquad \qquad \qquad = \frac{2D}{\lambda}3O_{13} \\
 & -2O_{2311}\dot{\gamma}_{11} + (O_{23} - 2O_{2322})\dot{\gamma}_{22} + (O_{23} - 2O_{2333})\dot{\gamma}_{33} \\
 & + (O_{13} - 4O_{2312})\dot{\gamma}_{12} + (O_{21} - 4O_{2313})\dot{\gamma}_{13} + (O_{33} + O_{22} - 4O_{2323})\dot{\gamma}_{23} \\
 & \qquad \qquad \qquad = \frac{2D}{\lambda}3O_{23}
 \end{aligned} \right\} \tag{5}$$

The example results of calculated orientation tensors of the second and

fourth orders based on the measured fibre orientations in the top, middle and bottom parts of the cylinder 1A are given in the Appendix A. The system of linear equations (5) for the components of the velocity gradient  $\dot{\gamma}_{ij}$  is solved for the ratio of  $\frac{\dot{\gamma}_{ij}\lambda}{D}$ . As the model parameter  $\frac{D}{\lambda}$  is not known, the results on the velocity gradients in different positions of the sample can be compared only relatively, i.e. as scaled velocity gradients.

## 5. Results

For each sample the components of the scaled velocity gradient  $\frac{\dot{\gamma}_{ij}\lambda}{D}$  have been calculated. The matrices are presented in Appendix B. For each velocity gradient matrix the eigenvalues and eigenvectors have been determined, Tables 1, 2, 3, 4, 5, 6. The eigenvector corresponding to the largest eigenvalue gives the direction of the largest change of velocity. A positive eigenvalue means an increase of velocity in that direction, and a negative eigenvalue shows that the flow velocity is decreasing in the direction of that eigenvector.

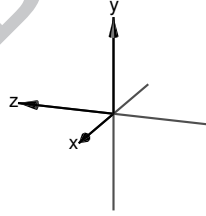


**Fig. 5.** The direction of the axes in visualisation of the eigenvectors received based on the velocity gradient matrices.

The following assumptions about the flow field of concrete mass can be made based on the measured fibre orientations and calculated velocity gradients:

- In the middle parts of the cylinders 1A, 1B, 2A, 2B there is a considerable difference between the largest and the smallest eigenvalue of the velocity gradient, Tables 1, 5. Two eigenvalues are of the same order of magnitude, whereas the third one is up to a factor of 20 smaller. This shows, that in one direction the velocity of concrete mass during the setting was almost constant, whereas in the perpendicular directions the velocity changed

considerably in space. The difference between the eigenvalues, as well as the value of the largest eigenvalue, is smaller in the other samples. This could indicate that compared with the other slabs the filling process for the slabs 1 and 2 was faster in the regions where the respective cylinders were extracted;

- In the middle parts of cylinders 1A, 2A, which are close to the boundary of the slab, Tables 1, 5, the direction of the largest velocity gradient is the z-direction, which was the average flow direction of concrete mass (Figure 3(a));
- In most of "A"-samples, (Figure 4), in the middle parts of cylinders 1A, 2A, 4A, 5A, Tables 1, 5, 3, 6, the eigenvector to the smallest eigenvalue is almost in the x-y-plane, i.e. the smallest variation of velocity of concrete mass is in the x-y-plane. This is the plane perpendicular to the average flow direction during the filling process;
- In "B"-samples, (Figure 4), in the middle parts of cylinders, the minimal velocity gradient is approximately in the y-direction. In this direction, the local velocity change is small;
- In "A"-samples close to the boundary, (Figure 4), the difference between the minimal and the maximal eigenvalue of the velocity gradient is more pronounced than in "B"-samples. In most cases, the maximal velocity gradient is larger in the "A"-samples than in the "B"-samples. Both results are reasonable due to the zero-slip condition at the boundary (zero velocity) and due to the influence of the boundary on fibre orientation;
- The velocity gradient in the samples taken from the top of the slab is much smaller than that in the samples taken from the bottom, Tables 1, 2, 3, 4. This is reasonable due to the influence of the solid formwork at the bottom, which enforces zero velocity at the boundary. On top there is a free surface, meaning no restrictions on the velocity.

**Table 1**

Eigenvalues and eigenvectors of velocity gradients in the top, middle and bottom parts of the cylinder 1A. Red line corresponds to vector  $\mathbf{x}_1$ , green line to vector  $\mathbf{x}_2$  and blue line to vector  $\mathbf{x}_3$ .

specimen	velocity gradient $(\nabla \mathbf{v})^{sym} \frac{\lambda}{D}$ in Cartesian components	visualisation	velocity gradient $(\nabla \mathbf{v})^{sym} \frac{\lambda}{D}$ in Spherical components
1A top	$\lambda_1 = -19.270, \mathbf{x}_1 = \begin{pmatrix} -0.621 \\ 0.778 \\ 0.922 \end{pmatrix}$ $\lambda_2 = 15.830, \mathbf{x}_2 = \begin{pmatrix} 0.749 \\ 0.555 \\ 0.361 \end{pmatrix}$ $\lambda_3 = 18.510, \mathbf{x}_3 = \begin{pmatrix} -0.230 \\ -0.293 \\ 0.928 \end{pmatrix}$		$\theta_1 = 23,$ $\phi_1 = 309$ $\theta_2 = 69,$ $\phi_2 = 37$ $\theta_3 = 22,$ $\phi_3 = 52$
1A middle	$\lambda_1 = -1.563, \mathbf{x}_1 = \begin{pmatrix} 0.711 \\ -0.703 \\ 0.015 \end{pmatrix}$ $\lambda_2 = 31.873, \mathbf{x}_2 = \begin{pmatrix} 0.645 \\ 0.660 \\ 0.386 \end{pmatrix}$ $\lambda_3 = 33.350, \mathbf{x}_3 = \begin{pmatrix} -0.260 \\ -0.244 \\ 0.851 \end{pmatrix}$		$\theta_1 = 89,$ $\phi_1 = 315$ $\theta_2 = 67,$ $\phi_2 = 46$ $\theta_3 = 32,$ $\phi_3 = 43$
1A bottom	$\lambda_1 = 95.850, \mathbf{x}_1 = \begin{pmatrix} -0.779 \\ 0.626 \\ 0.041 \end{pmatrix}$ $\lambda_2 = 117.370, \mathbf{x}_2 = \begin{pmatrix} -0.626 \\ -0.780 \\ 0.027 \end{pmatrix}$ $\lambda_3 = 125.320, \mathbf{x}_3 = \begin{pmatrix} 0.049 \\ -0.044 \\ 0.999 \end{pmatrix}$		$\theta_1 = 88,$ $\phi_1 = 321$ $\theta_2 = 88,$ $\phi_2 = 51$ $\theta_3 = 3,$ $\phi_3 = 318$

**Table 2**

Eigenvalues and eigenvectors of velocity gradients in the top, middle and bottom parts of the cylinder 1B. Red line corresponds to vector  $\mathbf{x}_1$ , green line to vector  $\mathbf{x}_2$  and blue line to vector  $\mathbf{x}_3$ .

specimen	velocity gradient $(\nabla \mathbf{v})^{sym} \frac{\lambda}{D}$ in Cartesian components	visualisation	velocity gradient $(\nabla \mathbf{v})^{sym} \frac{\lambda}{D}$ in Spherical components
1B top	$\lambda_1 = -0.057, \mathbf{x}_1 = \begin{pmatrix} -0.141 \\ -0.078 \\ 0.987 \end{pmatrix}$ $\lambda_2 = 0.493, \mathbf{x}_2 = \begin{pmatrix} -0.079 \\ 0.995 \\ 0.067 \end{pmatrix}$ $\lambda_3 = 5.500, \mathbf{x}_3 = \begin{pmatrix} 0.987 \\ 0.068 \\ 0.147 \end{pmatrix}$		$\theta_1 = 9,$ $\phi_1 = 29$ $\theta_2 = 86,$ $\phi_2 = 275$ $\theta_3 = 82,$ $\phi_3 = 4$
1B middle	$\lambda_1 = 2.833, \mathbf{x}_1 = \begin{pmatrix} 0.021 \\ 1.000 \\ 0.004 \end{pmatrix}$ $\lambda_2 = 12.957, \mathbf{x}_2 = \begin{pmatrix} 0.648 \\ -0.016 \\ 0.762 \end{pmatrix}$ $\lambda_3 = 22.760, \mathbf{x}_3 = \begin{pmatrix} -0.762 \\ 0.0136 \\ 0.648 \end{pmatrix}$		$\theta_1 = 90,$ $\phi_1 = 89$ $\theta_2 = 40,$ $\phi_2 = 359$ $\theta_3 = 50,$ $\phi_3 = 359$
1B bottom	$\lambda_1 = -47.013, \mathbf{x}_1 = \begin{pmatrix} 0.095 \\ -0.993 \\ 0.066 \end{pmatrix}$ $\lambda_2 = -10.226, \mathbf{x}_2 = \begin{pmatrix} -0.007 \\ 0.065 \\ 0.998 \end{pmatrix}$ $\lambda_3 = -4.614, \mathbf{x}_3 = \begin{pmatrix} 0.995 \\ 0.095 \\ 0.001 \end{pmatrix}$		$\theta_1 = 86,$ $\phi_1 = 275$ $\theta_2 = 4,$ $\phi_2 = 276$ $\theta_3 = 90,$ $\phi_3 = 5$

**Table 3**

Eigenvalues and eigenvectors of velocity gradients in the top, middle and bottom parts of the cylinder 4A. Red line corresponds to vector  $\mathbf{x}_1$ , green line to vector  $\mathbf{x}_2$  and blue line to vector  $\mathbf{x}_3$ .

specimen	velocity gradient $(\nabla\mathbf{v})^{sym} \frac{\lambda}{D}$ in Cartesian components	visualisation	velocity gradient $(\nabla\mathbf{v})^{sym} \frac{\lambda}{D}$ in Spherical components
4A top	$\lambda_1 = -19.075, \mathbf{x}_1 = \begin{pmatrix} -0.531 \\ 0.845 \\ 0.068 \end{pmatrix}$ $\lambda_2 = 2.269, \mathbf{x}_2 = \begin{pmatrix} 0.605 \\ 0.321 \\ 0.729 \end{pmatrix}$ $\lambda_3 = 4.059, \mathbf{x}_3 = \begin{pmatrix} -0.594 \\ -0.428 \\ 0.681 \end{pmatrix}$		$\theta_1 = 86,$ $\phi_1 = 302$ $\theta_2 = 43,$ $\phi_2 = 28$ $\theta_3 = 47,$ $\phi_3 = 36$
4A middle	$\lambda_1 = -7.032, \mathbf{x}_1 = \begin{pmatrix} 0.792 \\ -0.579 \\ 0.192 \end{pmatrix}$ $\lambda_2 = 18.560, \mathbf{x}_2 = \begin{pmatrix} 0.004 \\ 0.320 \\ 0.948 \end{pmatrix}$ $\lambda_3 = 21.706, \mathbf{x}_3 = \begin{pmatrix} -0.610 \\ -0.750 \\ 0.256 \end{pmatrix}$		$\theta_1 = 79,$ $\phi_1 = 324$ $\theta_2 = 19,$ $\phi_2 = 89$ $\theta_3 = 75,$ $\phi_3 = 51$
4A bottom	$\lambda_1 = -4.711, \mathbf{x}_1 = \begin{pmatrix} 0.608 \\ -0.710 \\ 0.356 \end{pmatrix}$ $\lambda_2 = 14.209, \mathbf{x}_2 = \begin{pmatrix} 0.622 \\ 0.704 \\ 0.343 \end{pmatrix}$ $\lambda_3 = 18.981, \mathbf{x}_3 = \begin{pmatrix} -0.494 \\ 0.013 \\ 0.870 \end{pmatrix}$		$\theta_1 = 69,$ $\phi_1 = 311$ $\theta_2 = 70,$ $\phi_2 = 49$ $\theta_3 = 30,$ $\phi_3 = 358$

**Table 4**

Eigenvalues and eigenvectors of velocity gradients in the top, middle and bottom parts of the cylinder 4B. Red line corresponds to vector  $\mathbf{x}_1$ , green line to vector  $\mathbf{x}_2$  and blue line to vector  $\mathbf{x}_3$ .

specimen	velocity gradient $(\nabla \mathbf{v})^{sym} \frac{\lambda}{D}$ in Cartesian components	visualisation	velocity gradient $(\nabla \mathbf{v})^{sym} \frac{\lambda}{D}$ in Spherical components
4B top	$\lambda_1 = -7.282, \mathbf{x}_1 = \begin{pmatrix} 0.345 \\ 0.839 \\ 0.421 \end{pmatrix}$ $\lambda_2 = 1.487, \mathbf{x}_2 = \begin{pmatrix} 0.013 \\ -0.453 \\ 0.892 \end{pmatrix}$ $\lambda_3 = 3.820, \mathbf{x}_3 = \begin{pmatrix} -0.939 \\ 0.302 \\ 0.167 \end{pmatrix}$		$\theta_1 = 65,$ $\phi_1 = 68$ $\theta_2 = 27,$ $\phi_2 = 272$ $\theta_3 = 80,$ $\phi_3 = 342$
4B middle	$\lambda_1 = 1.954, \mathbf{x}_1 = \begin{pmatrix} 0.062 \\ -0.993 \\ 0.096 \end{pmatrix}$ $\lambda_2 = 7.096, \mathbf{x}_2 = \begin{pmatrix} -0.124 \\ 0.103 \\ 0.987 \end{pmatrix}$ $\lambda_3 = 14.856, \mathbf{x}_3 = \begin{pmatrix} 0.990 \\ -0.049 \\ 0.130 \end{pmatrix}$		$\theta_1 = 84,$ $\phi_1 = 274$ $\theta_2 = 9,$ $\phi_2 = 320$ $\theta_3 = 83,$ $\phi_3 = 357$
4B bottom	$\lambda_1 = -23.593, \mathbf{x}_1 = \begin{pmatrix} 0.094 \\ -0.993 \\ 0.064 \end{pmatrix}$ $\lambda_2 = -5.133, \mathbf{x}_2 = \begin{pmatrix} -0.085 \\ 0.056 \\ 0.995 \end{pmatrix}$ $\lambda_3 = -2.290, \mathbf{x}_3 = \begin{pmatrix} 0.991 \\ 0.099 \\ 0.079 \end{pmatrix}$		$\theta_1 = 86,$ $\phi_1 = 275$ $\theta_2 = 6,$ $\phi_2 = 327$ $\theta_3 = 85,$ $\phi_3 = 6$

**Table 5**

Eigenvalues and eigenvectors of velocity gradients in the middle parts of the cylinders 2A, 2B, 3A, 3B. Red line corresponds to vector  $\mathbf{x}_1$ , green line to vector  $\mathbf{x}_2$  and blue line to vector  $\mathbf{x}_3$ .

specimen	velocity gradient $(\nabla \mathbf{v})^{sym} \frac{\lambda}{D}$ in Cartesian components	visualisation	velocity gradient $(\nabla \mathbf{v})^{sym} \frac{\lambda}{D}$ in Spherical components
2A middle	$\lambda_1 = -1.563, \mathbf{x}_1 = \begin{pmatrix} 0.771 \\ -0.703 \\ 0.015 \end{pmatrix}$ $\lambda_2 = 31.870, \mathbf{x}_2 = \begin{pmatrix} 0.645 \\ 0.660 \\ 0.386 \end{pmatrix}$ $\lambda_3 = 33.350, \mathbf{x}_3 = \begin{pmatrix} 0.281 \\ 0.265 \\ 0.922 \end{pmatrix}$		$\theta_1 = 89,$ $\phi_1 = 318$ $\theta_2 = 67,$ $\phi_2 = 46$ $\theta_3 = 23,$ $\phi_3 = 43$
2B middle	$\lambda_1 = 2.283, \mathbf{x}_1 = \begin{pmatrix} -0.056 \\ 0.998 \\ 0.006 \end{pmatrix}$ $\lambda_2 = 10.353, \mathbf{x}_2 = \begin{pmatrix} 0.003 \\ -0.005 \\ 0.100 \end{pmatrix}$ $\lambda_3 = 15.019, \mathbf{x}_3 = \begin{pmatrix} -0.998 \\ -0.056 \\ 0.003 \end{pmatrix}$		$\theta_1 = 90,$ $\phi_1 = 273$ $\theta_2 = 84,$ $\phi_2 = 301$ $\theta_3 = 90,$ $\phi_3 = 3$
3A middle	$\lambda_1 = -5.015, \mathbf{x}_1 = \begin{pmatrix} -0.493 \\ 0.514 \\ 0.702 \end{pmatrix}$ $\lambda_2 = -4.520, \mathbf{x}_2 = \begin{pmatrix} 0.859 \\ 0.163 \\ 0.485 \end{pmatrix}$ $\lambda_3 = -0.726, \mathbf{x}_3 = \begin{pmatrix} -0.134 \\ -0.842 \\ 0.522 \end{pmatrix}$		$\theta_1 = 45,$ $\phi_1 = 314$ $\theta_2 = 61,$ $\phi_2 = 11$ $\theta_3 = 59,$ $\phi_3 = 81$
3B middle	$\lambda_1 = -41.907, \mathbf{x}_1 = \begin{pmatrix} 0.154 \\ 0.661 \\ 0.735 \end{pmatrix}$ $\lambda_2 = -18.810, \mathbf{x}_2 = \begin{pmatrix} 0.519 \\ -0.687 \\ 0.509 \end{pmatrix}$ $\lambda_3 = -12.486, \mathbf{x}_3 = \begin{pmatrix} -0.841 \\ 0.303 \\ 0.449 \end{pmatrix}$		$\theta_1 = 43,$ $\phi_1 = 77$ $\theta_2 = 59,$ $\phi_2 = 307$ $\theta_3 = 63,$ $\phi_3 = 340$

**Table 6**

Eigenvalues and eigenvectors of the velocity gradient in middle parts of the cylinders 5A, 5B, 6A, 6B. Red line corresponds to vector  $\mathbf{x}_1$ , green line to vector  $\mathbf{x}_2$  and blue line to vector  $\mathbf{x}_3$ .

specimen	velocity gradient $(\nabla\mathbf{v})^{sym} \frac{\lambda}{D}$ in Cartesian components	visualisation	velocity gradient $(\nabla\mathbf{v})^{sym} \frac{\lambda}{D}$ in Spherical components
5A middle	$\lambda_1 = 0.143, \mathbf{x}_1 = \begin{pmatrix} -0.835 \\ 0.461 \\ 0.064 \end{pmatrix}$ $\lambda_2 = 15.704, \mathbf{x}_2 = \begin{pmatrix} -0.229 \\ -0.594 \\ 0.796 \end{pmatrix}$ $\lambda_3 = 21.472, \mathbf{x}_3 = \begin{pmatrix} 0.405 \\ 0.695 \\ 0.595 \end{pmatrix}$		$\theta_1 = 86,$ $\phi_1 = 331$ $\theta_2 = 37,$ $\phi_2 = 69$ $\theta_3 = 53,$ $\phi_3 = 60$
5B middle	$\lambda_1 = 14.667, \mathbf{x}_1 = \begin{pmatrix} -0.110 \\ -0.957 \\ 0.291 \end{pmatrix}$ $\lambda_2 = 20.178, \mathbf{x}_2 = \begin{pmatrix} -0.458 \\ 0.306 \\ 0.835 \end{pmatrix}$ $\lambda_3 = 23.556, \mathbf{x}_3 = \begin{pmatrix} 0.882 \\ 0.040 \\ 0.469 \end{pmatrix}$		$\theta_1 = 73,$ $\phi_1 = 83$ $\theta_2 = 33,$ $\phi_2 = 326$ $\theta_3 = 62,$ $\phi_3 = 3$
6A middle	$\lambda_1 = 3.442, \mathbf{x}_1 = \begin{pmatrix} 0.672 \\ -0.520 \\ 0.527 \end{pmatrix}$ $\lambda_2 = 7.501, \mathbf{x}_2 = \begin{pmatrix} -0.289 \\ 0.471 \\ 0.834 \end{pmatrix}$ $\lambda_3 = 12.717, \mathbf{x}_3 = \begin{pmatrix} -0.681 \\ -0.713 \\ 0.166 \end{pmatrix}$		$\theta_1 = 58,$ $\phi_1 = 322$ $\theta_2 = 33,$ $\phi_2 = 302$ $\theta_3 = 80,$ $\phi_3 = 46$
6B middle	$\lambda_1 = -50.793, \mathbf{x}_1 = \begin{pmatrix} -0.245 \\ -0.874 \\ 0.423 \end{pmatrix}$ $\lambda_2 = -37.816, \mathbf{x}_2 = \begin{pmatrix} -0.350 \\ 0.486 \\ 0.801 \end{pmatrix}$ $\lambda_3 = -20.104, \mathbf{x}_3 = \begin{pmatrix} 0.904 \\ -0.048 \\ 0.424 \end{pmatrix}$		$\theta_1 = 65,$ $\phi_1 = 74$ $\theta_2 = 37,$ $\phi_2 = 306$ $\theta_3 = 65,$ $\phi_3 = 357$

## 6. Discussion

The possible reasons why the estimated velocity gradients differ from each other in the different floor slabs may be:

- Usually, during the placing the fresh SCC behaves as a fluid. However, when it is cast slowly enough or if it is at rest, it flocculates and builds up an internal structure, and has the ability to withstand a load coming from the concrete mass casting above, without increasing the lateral stress against the formwork [18]. During the production of full-size floor slabs the casting conditions might have been different;
- The casting process used to produce the slabs was a multi-layer or distinct layers casting (Figure 2). During the placing, a layer of SCC has a short time to rest and flocculates before a second layer of concrete is cast above it. If it flocculates too much and its apparent yield stress increases above a critical value, then the two layers do not mix at all, and this creates a weak interface in the final structure. The fact that the full-size floor slabs 4,5 and 6 were weaker in the bending test [16, 17], might indicate that in these slabs there was insufficient mixing of concrete mass between the layers formed by the casting order represented in Figure 2. This correlated with the observations, that in cylinders 1 and 2 the largest velocity gradient was calculated, which may support an assumption that the casting of the slabs 1 and 2 was faster compared to the other ones;
- In the case of cementitious composites the amount of fibres added to the mass is usually sufficient to create the interactions between fibres, such as direct contacts or hydrodynamic interactions. When the length of fibres is of the same order as the maximum aggregate size, fibre orientations will be dictated by the random contact interactions between grains and fibres. This is an additional randomising effect. All these additional interactions are important for the final orientation of fibres, but are not taken into account in the Jeffrey model. This may lead to deviations between the theoretical predictions and experimental results.

The model equation (4) is simplified in several aspects, such as:

- The anti-symmetric part of the velocity gradient has been neglected, but it is not clear, if this is justified during the filling process;
- Fibre-fibre interactions have not been taken into account. Such interactions would lead to terms nonlinear in the orientation tensor. Fibre-grain interactions may also be relevant.

## 7. Conclusion

The present study gives a first idea about the trends of flow dynamics of concrete mass with steel fibres during the filling process. The approach presented leads to a set of linear algebraic equations for the components of the velocity gradient, meaning that no numerical methods are needed. The model equation (4) allowed to calculate the scaled velocity gradients of concrete mass  $(\nabla\mathbf{v})^{sym} \frac{\lambda}{D}$  based on fibre orientations measured in the hardened concrete samples taken from the different regions in the slabs. The results lead to a comparison of the magnitude of the velocity gradients in different regions, and they demonstrate, in which direction the change of velocity of concrete mass is large and in which direction it is small.

As the measuring of fibre orientations during the flow of concrete mass is hardly feasible then the approach proposed can be used f.i. to interpolate the orientation of fibres between two time moments with the known fibre orientations. If the casting is made by pump tube then at a time moment corresponding to the start of casting, the fibres are aligned with flow direction of concrete mass in the pipe, and their orientation is known. The final time moment corresponds to a steady state, when the concrete mass has set and fibre orientations are frozen, and can be measured. By knowing the orientation of fibres at these two time moments it is possible to interpolate the orientation of fibres using the equation (1). Fibre orientations interpolated between two time moments with the known fibre orientations is a subject of future studies.

## Author contributions

Both authors contributed equally to the research, discussions and writing this article.

### Acknowledgements

One of us (C.P.) gratefully acknowledges support by the "Berliner Chancengleichheitsprogramm" (BCP). For ME the research leading to these results has received funding from the Academy of Finland Post-doctoral Researcher" grant number 289740. We would like to thank Prof. Jari Puttonen for valuable discussions and comments.

### Data Availability

The raw/processed data required to reproduce these findings cannot be shared at this time due to technical limitations.

### References

- [1] Alberti MG, Enfedaque A, Gálvez JC (2018) A review on the assessment and prediction of the orientation and distribution of fibres for concrete. *Composites Part B: Engineering*, 151:274–290.
- [2] Chand S (2000) Review carbon fibers for composites. *Journal of Materials Science*, 35(6):1303–1313.
- [3] Blau WJ, Coleman N, Kahn U, Gunko YK (2006) Small but strong: A review of the mechanical properties of carbon nanotube-polymer composites. *Carbon*, 44(9):1644–1652
- [4] Eik M, Puttonen J, Herrmann H (2014) An orthotropic material model for steel fibre reinforced concrete based on the orientation distribution of fibres. *Composite Structures*, 121:324–336
- [5] Herrmann H, Eik M, Berg V, Puttonen J (2014) Phenomenological and numerical modelling of short fibre reinforced cementitious composites. *Mechanica*, 49:1985–2000
- [6] Fan Z, Advani SG (2005) Characterization of orientation state of carbon nanotubes in shear flow. *Polymer*, 46(14):5232–5240
- [7] Kang DW, Ryu SH (2013) Orientation of carbon nanotubes in polypropylene melt. *Polymer International*, 62(2):152–157

- [8] Sulong AB, Park J (2011) Alignment of multi-walled carbon nanotubes in a polyethylene matrix by extrusion shear flow: mechanical properties enhancement. *J Composite Materials*, 45(8):931–941
- [9] Pujari S, Rahatekar S, Gilman J, Koziol K, Windle A, Burghardt W (2009) Orientation dynamics in multiwalled carbon nanotube dispersions under shear flow. *J Chem Phys*, 130:214903–214912
- [10] Pötschke P, Fornes T, Paul D (2002) Rheological behavior of multiwalled carbon nanotube/polycarbonate composites. *Polymer*, 43:3247–3255
- [11] Kröger M, Hess S (1993) Viscoelasticity of polymeric melts and concentrated solutions. The effect of flow-induced alignment of chain ends. *Physica A*, 195:336–353
- [12] Ilg P, Kröger M, Hess S (2002) Magnetoviscosity and orientational order parameters of dilute ferrofluids. *Journal of Chemical Physics*, 116(20):9078–9088
- [13] Ehrentraut H, Chrzanowska A (2013) Induced anisotropy in rapid flows of nonspherical granular materials. *Lecture Notes in Applied and Computational Mechanics*, 11:343–364
- [14] Advani S, Tucker C (1987) The use of tensors to describe and predict fiber orientation in short fiber composites. *J Rheol*, 31:751–784
- [15] Suuronen JP, Kallonen A, Eik M, Puttonen J, Serimaa K, Herrmann H (2013) Analysis of short fibres orientation in steel fibre reinforced concrete (SFRC) using x-ray tomography. *Journal of Materials Science*, 48(3):1358–1367
- [16] Eik M (2014) Orientation of short steel fibres in concrete: measuring and modelling. Doctoral dissertation
- [17] Eik M, Löhmus K, Tigasson M, Listak M, Puttonen J, Herrmann H (2013) DC-conductivity testing combined with photometry for measuring fibre orientations in SFRC. *Journal of Materials Science*, 48(10):3745–3759

- [18] Editors: Roussel N, Gram, A(2014)Simulation of Fresh Concrete Flow. State-of-the Art Report of the RILEM Technical Committee 222-SCF. RILEM State-of-the-Art Reports A
- [19] Scheuer A, Amar A, Abisset-Chavanne A, Cueto E, Chinesta F, Keunings R, Advani S(2018) Data-driven upscaling of orientation kinematics in suspensions of rigid fibres. Computer Modeling in Engineering and Sciences, 117(3):367–386

**Appendix A. OTs of the second and fourth orders for the top, middle and bottom parts of the cylinder 1A**

Second order orientation tensors  $O_{ij}$

Top part

Middle part

Bottom part

$$\begin{pmatrix} 0.34 & 0.24 & -0.10 \\ 0.24 & 0.23 & -0.15 \\ -0.10 & -0.15 & 0.43 \end{pmatrix}; \begin{pmatrix} 0.20 & 0.16 & -0.11 \\ 0.16 & 0.21 & -0.12 \\ -0.11 & -0.12 & 0.59 \end{pmatrix}; \begin{pmatrix} 0.10 & 0.09 & 0.09 \\ 0.09 & 0.14 & 0.12 \\ 0.09 & 0.12 & 0.76 \end{pmatrix};$$

Fourth order orientation tensors  $O_{ijkl}$ 

Top part	Middle part			Bottom part				
$O_{ij11} =$	$O_{ij11} =$			$O_{ij11} =$				
0.178	0.114	-0.038	0.078	0.055	-0.028	0.027	0.021	0.015
0.114	0.088	-0.036	0.055	0.050	-0.026	0.021	0.025	0.015
-0.038	-0.036	0.073	-0.028	-0.026	0.071	0.015	0.015	0.049
$O_{ij21} =$	$O_{ij21} =$			$O_{ij21} =$				
0.114	0.088	-0.036	0.055	0.050	-0.026	0.021	0.025	0.015
0.088	0.075	-0.033	0.050	0.052	-0.027	0.025	0.033	0.015
-0.036	-0.033	0.049	-0.026	-0.027	0.052	0.015	0.015	0.031
$O_{ij31} =$	$O_{ij31} =$			$O_{ij31} =$				
-0.038	-0.036	0.073	-0.028	-0.026	0.071	0.015	0.015	0.049
-0.036	-0.033	0.049	-0.026	-0.027	0.052	0.015	0.015	0.031
0.073	0.049	-0.032	0.071	0.052	-0.055	0.049	0.031	0.062
$O_{ij12} =$	$O_{ij12} =$			$O_{ij12} =$				
0.114	0.088	-0.036	0.055	0.050	-0.026	0.021	0.025	0.015
0.088	0.075	-0.033	0.050	0.052	-0.027	0.025	0.033	0.015
-0.036	-0.033	0.049	-0.026	-0.027	0.052	0.015	0.015	0.031
$O_{ij22} =$	$O_{ij22} =$			$O_{ij22} =$				
0.088	0.075	-0.033	0.050	0.052	-0.027	0.025	0.033	0.015
0.075	0.081	-0.042	0.052	0.089	-0.030	0.033	0.058	0.025
-0.033	-0.042	0.066	-0.027	-0.030	0.072	0.015	0.025	0.056
$O_{ij32} =$	$O_{ij32} =$			$O_{ij32} =$				
-0.036	-0.033	0.049	-0.026	-0.027	0.052	0.015	0.015	0.031
-0.033	-0.042	0.066	-0.027	-0.030	0.072	0.015	0.025	0.056
0.049	0.066	-0.071	0.052	0.072	-0.069	0.031	0.056	0.080
$O_{ij13} =$	$O_{ij13} =$			$O_{ij13} =$				
-0.038	-0.036	0.073	-0.028	-0.026	0.071	0.015	0.015	0.049
-0.036	-0.033	0.049	-0.026	-0.027	0.052	0.015	0.015	0.031
0.073	0.049	-0.032	0.071	0.052	-0.055	0.049	0.031	0.062
$O_{ij23} =$	$O_{ij23} =$			$O_{ij23} =$				
-0.036	-0.033	0.049	-0.026	-0.027	0.052	0.015	0.015	0.031
-0.033	-0.042	0.066	-0.027	-0.030	0.072	0.015	0.025	0.056
0.049	0.066	-0.071	0.052	0.072	-0.069	0.031	0.056	0.080
$O_{ij33} =$	$O_{ij33} =$			$O_{ij33} =$				
0.073	0.049	-0.032	0.071	0.052	-0.055	0.049	0.031	0.062
0.049	0.066	-0.071	0.052	0.072	-0.069	0.031	0.056	0.080
-0.032	-0.071	0.289	-0.055	-0.069	0.448	0.062	0.080	0.655

## Appendix B. Calculated velocity gradients in different samples

**Table B.7**

The components of the symmetric part of the velocity gradient

specimen	velocity gradient $(\nabla \mathbf{v})^{sym} \frac{\lambda}{D}$ in Cartesian components	specimen	velocity gradient $(\nabla \mathbf{v})^{sym} \frac{\lambda}{D}$ in Cartesian components
1A top	$\begin{pmatrix} 2.417 & 17.150 & 1.440 \\ 17.150 & -5.187 & -3.248 \\ 1.440 & -3.248 & 17.839 \end{pmatrix}$	1B top	$\begin{pmatrix} 5.358 & 0.330 & 0.801 \\ 0.330 & 0.513 & 0.092 \\ 0.801 & 0.092 & 0.065 \end{pmatrix}$
1A middle	$\begin{pmatrix} 15.098 & 16.823 & -0.749 \\ 16.823 & 15.440 & 0.001 \\ -0.749 & 0.001 & 33.122 \end{pmatrix}$	1B middle	$\begin{pmatrix} 18.636 & -0.308 & -4.838 \\ -0.308 & 2.839 & 0.049 \\ -4.838 & 0.049 & 17.074 \end{pmatrix}$
1A bottom	$\begin{pmatrix} 104.340 & 10.490 & 1.067 \\ 10.490 & 108.930 & -0.583 \\ 1.067 & -0.583 & 125.270 \end{pmatrix}$	1B bottom	$\begin{pmatrix} -4.998 & 4.010 & -0.224 \\ 4.010 & -46.470 & 2.398 \\ -0.224 & 2.398 & -10.384 \end{pmatrix}$
2A middle	$\begin{pmatrix} 15.098 & 16.823 & -0.749 \\ 16.823 & 15.440 & 0.001 \\ -0.749 & 0.001 & 33.122 \end{pmatrix}$	2B middle	$\begin{pmatrix} 14.979 & 0.711 & -0.011 \\ 0.711 & 2.323 & -0.046 \\ -0.011 & -0.046 & 10.353 \end{pmatrix}$
3A middle	$\begin{pmatrix} -4.572 & 0.555 & -0.095 \\ 0.555 & -1.960 & -1.847 \\ -0.095 & -1.847 & -3.729 \end{pmatrix}$	3B middle	$\begin{pmatrix} -14.892 & -0.742 & -5.004 \\ -0.742 & -28.309 & -2.071 \\ -5.004 & -2.071 & -30.003 \end{pmatrix}$
4A top	$\begin{pmatrix} -3.117 & 10.027 & 0.050 \\ 10.027 & -12.630 & -1.753 \\ 0.050 & -1.753 & 3.000 \end{pmatrix}$	4B top	$\begin{pmatrix} 2.501 & -3.197 & -1.638 \\ -3.197 & -4.474 & -2.980 \\ -1.638 & -2.980 & -0.003 \end{pmatrix}$
4A middle	$\begin{pmatrix} 3.677 & 13.185 & -4.385 \\ 13.185 & 11.737 & 2.246 \\ -4.385 & 2.246 & 17.821 \end{pmatrix}$	4B middle	$\begin{pmatrix} 14.687 & -0.690 & 1.029 \\ -0.690 & 2.040 & 0.443 \\ 1.029 & 0.443 & 7.179 \end{pmatrix}$
4A bottom	$\begin{pmatrix} 8.386 & 8.133 & -6.138 \\ 8.133 & 4.669 & 4.833 \\ -6.138 & 4.833 & 15.423 \end{pmatrix}$	4B bottom	$\begin{pmatrix} -2.499 & 2.005 & 0.112 \\ 2.005 & -23.326 & 1.199 \\ 0.112 & 1.199 & -5.192 \end{pmatrix}$
5A middle	$\begin{pmatrix} 4.452 & 7.966 & -2.271 \\ 7.966 & 15.188 & 1.924 \\ -2.271 & 1.924 & 17.680 \end{pmatrix}$	5B middle	$\begin{pmatrix} 22.742 & -0.452 & 1.571 \\ -0.452 & 15.198 & 1.578 \\ 1.571 & 1.578 & 20.461 \end{pmatrix}$
6A middle	$\begin{pmatrix} 8.088 & 3.952 & -2.029 \\ 3.952 & 9.055 & 0.494 \\ -2.029 & 0.494 & 6.518 \end{pmatrix}$	6B middle	$\begin{pmatrix} -24.109 & -3.532 & 8.136 \\ -3.532 & -47.663 & 4.426 \\ 8.136 & 4.426 & -36.941 \end{pmatrix}$